

Development of extreme ultraviolet scatterometer using multiple orders of high-harmonic generation

Yi-Sha Ku
Wei-Ting Wang
Yi-Chang Chen
Ming-Chang Chen
Chia-Liang Yeh
Chun-Wei Lo

Development of extreme ultraviolet scatterometer using multiple orders of high-harmonic generation

Yi-Sha Ku,^{a,b,*} Wei-Ting Wang,^{a,b} Yi-Chang Chen,^{a,c} Ming-Chang Chen,^b Chia-Liang Yeh,^a and Chun-Wei Lo^a

^aIndustrial Technology Research Institute, Center for Measurement Standards, Hsinchu, Taiwan

^bNational Tsing Hua University, Institute of Photonics Technologies, Hsinchu, Taiwan

^cNational Tsing Hua University, Department of Power Mechanical Engineering, Hsinchu, Taiwan

Abstract. We developed an extreme ultraviolet (EUV) scatterometer equipped with a table-top EUV source for the characterization of nanoscale grating lines. Appropriate orders of high-harmonic generation at wavelengths ranging from 25 to 35 nm are selected as the coherent light source for high-resolution spatial performance. It is shown that the grating surface profile significantly affects the scattered diffraction intensities and can be retrieved by the structure reconstruction algorithms using inverse modeling by rigorous coupled wave analysis. © *The Authors*. Published by SPIE under a Creative Commons Attribution 3.0 Unported License. Distribution or reproduction of this work in whole or in part requires full attribution of the original publication, including its DOI. [DOI: [10.1117/1.JMM.17.1.014001](https://doi.org/10.1117/1.JMM.17.1.014001)]

Keywords: scatterometer; high-harmonic generation; rigorous coupled wave analysis.

Paper 17121 received Sep. 1, 2017; accepted for publication Feb. 5, 2018; published online Feb. 24, 2018.

1 Introduction

Scatterometry is an optical metrology technique designed for analyzing the changes of light intensity in a device. This technique is widely used for the wafer metrology of nanostructured surfaces in the semiconductor industry. There are two conventional scatterometric approaches: angle-resolved and specular spectroscopic scatterometer.^{1,2} Angle-resolved scatterometry involves single-wavelength readings at various angles, which has several moving parts and therefore requires careful adjustment and alignment of the components. The scatterometers used in the semiconductor industry are typically specular spectroscopic systems, which work at a fixed angle of incidence but in broadband wavelengths range in the visible or UV, and measure only the zeroth-order diffraction. The complex refractive indices of the structure and substrate materials have to be known over a broad wavelength range, which becomes a difficulty of many material applications in advanced process. In contrast to variable-angle and specular spectroscopic scatterometries, the proposed extreme ultraviolet (EUV) scatterometer is designed to measure the intensity of nonzerth-order diffraction at a fixed incident angle and at multiple laser-like wavelengths. The short wavelengths of EUV, which give rise of several diffraction orders of scattering from nanoscale grating features, will increase measurement sensitivity and allows accurate extraction of topographic profile information from periodic structures with dimensions smaller than submicrons.^{3,4}

Scatterometry is a model-based approach that involves comparing light-scattering measurements against theoretical “signature” scatter patterns. In the forward problem, a theoretical model uses a rigorous grating theory to determine a series of diffraction efficiencies that correspond to discrete iterations of various grating parameters. The inverse problem is solved by the analysis of the measured diffraction efficiency signatures when finding the best match to the pre-generated library data. We extend earlier scatterometry work

by employing nonzerth-order diffracted light and polychromatic wavelengths of high-harmonic generation (HHG) in the EUV range for increasing the measurement sensitivities on grating parameters. High-harmonic (HH) emission consisting of a few harmonic orders, namely 15 to 50 nm, was selected to illuminate periodic structures for diffractive imaging. It was shown that it is feasible to characterize the periodic structures for critical dimension (CD) and other profile properties by means of rigorous numerical modeling.^{5,6}

In this study, we demonstrate the most straightforward geometrical setup by simply illuminating the sample along an incidence angle of 45 deg, an approach of reflection mode EUV scatterometer. Our previous system, which fixed the distance between the grating and the CCD sensor at 157.4 mm, imposed the large diffraction angles of both of the $m = \pm 1$ beams diffracted from grating sample with high density of 7200 lines/mm needs to be measured separately by rotating the sample to the appropriate incident angles to fit in the CCD window.⁷ However, herein, we have modified the previous system by placing a vacuum compatible CCD camera inside the scatterometer chamber. A microscopic translation stage, for mounting the CCD, was designed to adjust the distance between the grating target and the CCD detector in a range of 25.0 to 40.5 mm. This allows both the $m = +1$ and -1 diffracted beams to be directly and simultaneously collected by the CCD camera with maximal spatial resolution. The intensity distribution of the far-field diffraction pattern can be corrected through a coordinate transformation, in which the propagation distance of each harmonic from the sample to detector planes is equal. The corrected diffraction intensity also allows the accurate extraction of topographic profile information. The comparison with CD measurements using a cross-sectional scanning electron microscope (SEM) showed a good correlation of the results.

2 Samples and Instrumentation

2.1 Sample Details

The sample consists of a rectangular reflection grating with a density of approximately 7200 lines/mm, a nominal

*Address all correspondence to: Yi-Sha Ku, E-mail: yku@itri.org.tw

groove depth of 50 nm, and etched by a single-crystal silicon substrate. A square of size 12.5 mm was used for study.

2.2 HHG Source

High-order harmonics are generated by focusing a single-unit integrated femtosecond (fs) laser (Pharos, Light-Conversion) beam into an argon-filled gas cell.⁸ A solid-state laser diode was used for pumping an Yb medium. This provides a 170-fs pulse duration, 1.5 mJ of pulse energy, 6 W of average power, and a 4 kHz repetition rate at the central wavelength of 1030 nm. The EUV radiation emission consists of distinct spectral components given by odd high-order harmonics of the fundamental frequency and displays collimated laser-like characteristics. The parallel polychromatic beam incident on a grating disperses the light where each wavelength in the input-beam spectrum is diffracted in a different direction. This produces a spatially separated spectrum satisfying the grating equation. Thus, the wavelengths of the high-order harmonics generated and the accurate grating pitch were confirmed by the spatial distributions captured by the CCD camera. This is based on the known incident angle and the sample-CCD distance. Previous research showed that high-order harmonics can be tailored and confined to only a few orders, depending on the experimental requirements, by an appropriate choice of gas species and pressure, laser-focus position, the laser-beam intensity and diameter, and the length of gas cell.^{9,10}

2.3 Scatterometer Design

The design of the EUV scatterometer module is similar to the system reported in a previous study.⁷ The experimental geometry is outlined in Fig. 1. The EUV scatterometer system consists of a 20-cm lens for focusing incident light, an Ar gas cell, three Al filters, a pair of Kirkpatrick–Baez (K–B) mirrors, a grating-structure sample, and a back-illuminated CCD camera. The argon-filled gas cell enables HHG in the bright line region of 25 to 35 nm. Al filters, consisting of three 200-nm-thick Al layers, were inserted to block 1030 nm pump light. The K–B mirror pairs focused on the HH beam to spot sizes below 100 μm . A closed-up of the opened scatterometer chamber is shown in Fig. 2. The reflection grating sample was placed around a 45 deg angle of incidence near the focus of the EUV beam. The sample holder was mounted onto a piezoelectric x - y - z - θ stage, with a range of ± 21 mm, a linear resolution of 1 nm, and

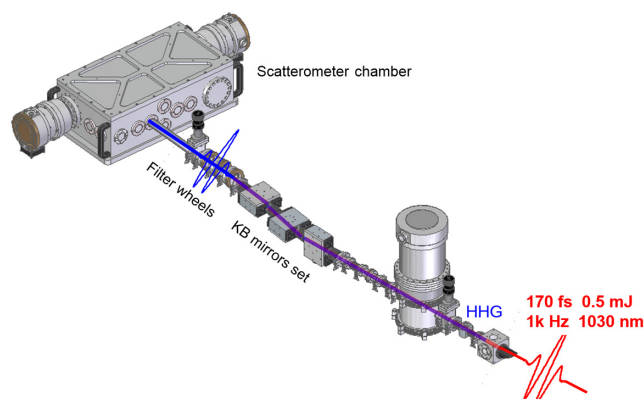


Fig. 1 Schematic of the EUV scatterometer.

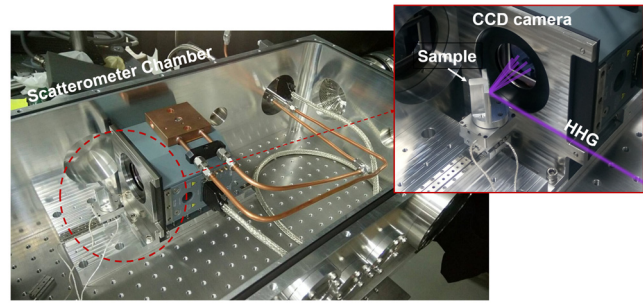


Fig. 2 Closed-up of the opened EUV scatterometer chamber.

a rotational resolution of $2 \text{ deg} \times 10^{-4}$. A vacuum compatible CCD camera (Andor DX420) with 1024×256 array and pixel size $26 \mu\text{m} \times 26 \mu\text{m}$ was placed on a longitudinal translation stage with an adjustable distance of 25.0 to 40.5 mm away from the sample to capture the diffraction pattern in an optimization condition, oriented with its surface nearly normal to the zero-order diffraction of the beam. The CCD camera recorded the diffraction and scattering intensity images in a straightforward manner, without requiring any intermediary imaging optics. The angular field-of-view in the cross dispersion direction is determined by the width of the CCD window and the distance to the sample.

3 Theoretical Model and Measurement Algorithm

3.1 Grating Equation for HHG Wavelengths Calibration

The HHG output coupled EUV beam contains many superimposed harmonics. The nanoscale periodic geometrical structures serve as an optical grating to separate the harmonics onto the CCD camera. The position of the dispersed diffraction spectra on the detector gives the wavelength through the grating equation

$$\pm m\lambda_n = d[\sin \theta_i + \sin \theta_{\pm m}(\lambda_n)], \quad (1)$$

where m is an integer that specifies the order of diffraction, $\lambda_n = \lambda_0/n$ is the wavelength of the n 'th order of HHG, λ_0 is the fundamental wavelength, d is the grating pitch, θ_i is the angle of HH beam incidence onto the grating surface, and $\theta_{\pm m}$ are the diffracted angles corresponding to the set of discrete HH wavelengths at diffraction orders $\pm m$. Positive and negative orders of diffraction occurred on both sides of the zero-order beam.

3.2 Theoretical Model of Grating-Diffraction Response of HHG

We used rigorous coupled wave theory, one of the most versatile and robust models used for computing diffraction effects in mono- and multilayer gratings.^{11,12} It uses film stack information (optical refractive indices and thickness values) and the grating parameters (height and profile characteristics) to theoretically predict diffraction from the measured structure. The complex refractive indices of the grating structure and substrate materials in the EUV range are calculated based on the Center for X-ray Optics database. A staircase approximation for nonrectangular gratings graded along the z -direction is used in RCWA to predict the grating efficiency accurately for a wide variety of grating profiles

over wide spectral ranges. The electromagnetic modes in each layer are calculated and analytically propagated through the layers. The distribution of the incident field power at a given wavelength, diffracted by the grating sample into the various orders, depends on many parameters. These parameters include the incident power, the incidence and diffraction angles, the refractive index of the grating material, and the grating profile. The extraction of the latter can be viewed as an optimization problem, yielding the best agreement between theory and measurement, to enable three-dimensional (3-D) structure profile reconstruction.

3.3 Diffraction Intensities Correction

Scattering geometries for nominal 45 deg incidence angles are shown in Fig. 3. x is the detector array coordinates and R is the distance from the sample to the center of the detector. The intensities recorded on the flat detector were distorted due to the nonequal distances of each harmonic along their diffraction angles onto the flat detector. Because the intensity falls off as $1/r_i^2$, we rescale the measured diffraction intensity data by r_i^2/R^2 to map the flat detector coordinate back to the Ewald sphere, E . Here, r_i is the distance from the sample to a given pixel x_i on the detector.¹³ When written in terms of detector coordinates, we have $1 + x_i^2/R^2$. To summarize the intensity correction steps, we start with the measured diffraction pattern intensity, $I(x_i)$, in terms of the detector coordinates. We then perform the intensity rescaling as

$$I_E(r_i) = \left(1 + \frac{x_i^2}{R^2}\right) I(x_i),$$

where I_E is now properly rescaled on the Ewald sphere and is ready to be further integrated for library comparison.

3.4 Library Match Process

To solve the inverse problem, once the HHG wavelengths are determined through the calibration process as discussed in Sec. 3.1, a library of HHG scatter signatures spanning a range of CD values, grating depths, and side-wall angles is pregenerated as described in Sec. 3.2. This library is then searched to find the best match to corrected measurement data as interpreted in Sec. 3.3.

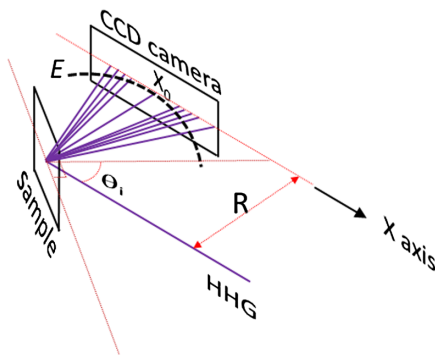


Fig. 3 Scattering geometries of EUV scatterometer. R is the normal distance from the sample to the center of the detector. The experimental diffraction pattern is a result of mapping HHG from the Ewald sphere onto a flat detector.

4 Results and Discussions

4.1 HHG Wavelengths Determination

Figure 4(a) outlines the geometrical arrangement of the grating sample and CCD detector. An etched silicon reflection grating of density 7200 lines/mm and nominal depth 50 nm was used for the test. The EUV beam was incident at a nominal angle $\theta_i = 45.0$ deg onto the grating surface. The distance between the grating and the CCD sensor was adjusted at 27.0 mm, which is just about the optimal distance allowing both of the $m = \pm 1$ diffraction beams to fit into the CCD window simultaneously. The sample positioner was equipped with a x - y - z - θ stage to move and rotate the sample into the EUV beam focus. The beam focus was made to coincide exactly with the axis of rotation. The upper section of Fig. 4(b) shows the diffraction image, as viewed in the CCD window, which allows the $m = \pm 1$ diffraction intensities to be acquired simultaneously. The CCD exposure time was 30 s. The lower panel plots the total CCD counts and summed vertically along each column of pixels. Four of the wavelengths corresponding to the orders of $n = 33$ rd, 35th, 37th, and 39th HHG can be derived from the same grating equation, according to the discrete diffracted angles of θ_{+1} and θ_{-1} .

Table 1 shows the calculated HHG orders and wavelengths based on the grating equation [Eq. (1)]. Some parameters such as the fundamental wavelength λ_0 , incident angle θ_i , grating pitch d , and sample-to-CCD distance R are common to the whole set of four independent grating equations.

The diffraction angles were calculated from arctangent of $|x_i - x_0|/R$, where $|x_i - x_0|$ is the distance between the diffraction peaks ($m = \pm 1$) and the CCD center. Thanks to many distinct harmonic orders, the greater the number of independent grating equations, the more parameters can be fitted. Thus, the fundamental wavelength, incident angle, and sample-to-CCD distance are confirmed to be 1027 nm, 41.87 deg, and 26.88 mm, respectively. This minimizes the fitting errors on the HHG orders and wavelengths.

4.2 Library Generation and Matching Process

The HHG wavelengths of 31.12, 29.34, 27.76, and 26.33 nm, which correspond to the harmonics order of 33rd, 35th, 37th, and 39th, respectively, have been determined by fitting the grating equations with their well-separated positions of $m = \pm 1$ diffraction beams. Those four HHG wavelengths are separately used to model each individual characteristic signature of diffraction efficiencies for varying grating CDs, depths, and side-wall angles, respectively. We create full range libraries (CD ranges from 60.0 to 80.0 nm in an increment step of 0.1 nm, depth from 40.0 to 60.0 nm in an increment step of 0.1 nm, side-wall angle from 85.00 deg to 90.00 deg in a step of 0.01 deg) to be searched and find the best match to the measured data. The approach to include more harmonics for library generation and matching substantially enhance the measurement accuracy and ensures that the solution of the complex parameters is unique. The parameters correlation issues can be minimized as well.

We rescale the measured diffraction intensity data by $1 + x_i^2/R^2$ to map the flat detector coordinate back to the Ewald sphere, as discussed in Sec. 3.3. The most accurate

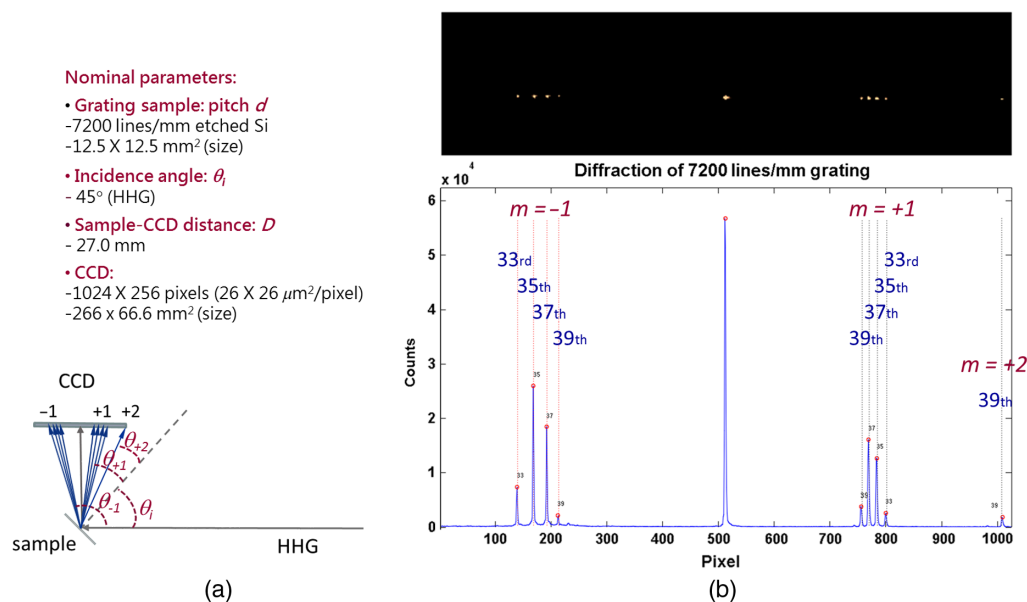


Fig. 4 (a) Schematic diagram of the geometrical arrangement of the EUV scatterometry experiment. (b) Measured diffraction image spectrum from an etched silicon reflection grating with a density of 7200 lines/mm together with the best fitting results (red dots) using the laser and geometry parameters listed in Tables 1 and 2. The upper section is the diffraction image, as viewed in the CCD window. The lower panel plots the total CCD counts summed vertically along each column of 1024 pixels.

Table 1 HHG orders and wavelength calibration.

λ_0 (nm)	Incident angle (deg)	Pitch (L/mm)	R (mm)	HH order	HH		Diff. angle (deg)	
					λ (nm)	$m = -1$	$m = +1$	
1027	41.87	7200	26.88	33rd	31.12	-63.04	-26.31	
				35th	29.34	-61.46	-27.13	
				37th	27.76	-60.12	-27.87	
				39th	26.33	-58.96	-28.53	

measurements of diffraction intensities require many counts under the peaks. The intensity counts are integrated over a small angular range and an estimated background, which is 2% of the integrated counts, is subtracted from the enclosed area. To eliminate pulse-to-pulse laser-intensity fluctuations, which can in turn cause HHG peak intensity fluctuations, the

Table 2 7200 lines/mm etched silicon grating match results.

HH order	HH λ (nm)	Exp. intensity		Exp. ratio (-1/+1)	Theo. ratio (-1/+1)	% variation
		$m = -1$	$m = +1$			
33rd	31.12	1,009,198	683,592	1.48	4.25	-0.65
35th	29.34	1,922,189	2,087,900	0.92	1.33	-0.31
37th	27.76	1,307,548	2,729,359	0.48	0.46	0.05
39th	26.33	339,611	965,103	0.35	0.46	0.23

ratio of first-order ($m = +1$ to $m = -1$) reflectivity is calculated and used for library matching. Table 2 lists the detailed counts under each HHG diffraction peak and the best-match results between the measurement and modeling. A metric of percentage variation allows a comparison of the theoretical and measured diffraction efficiencies in individual orders of HHG. Figure 5(a) shows the reconstructed grating profile based on the parameters including the top CD, bottom CD, and grating depth generated to obtain the best match. The model fit for a top CD of 68.5 nm, a bottom CD of 75.0 nm, and a grating depth of 50.0 nm shows satisfactory agreement with the cross-sectional SEM result provided by the grating manufacturer (LightSmyth) as shown in Fig. 5(b). An argument about our current model calculated a series of diffraction efficiencies that correspond to discrete iterations of various grating parameters in a 0.1-nm step, which might not as precise as the cross-sectional SEM shown with 0.01-nm accuracy. However, it is important to note that it would be a good tool for nondestructive characterization, which the SEM cannot offer, and in particular, for inline process control of fabrication.

5 Summary

We developed an EUV scatterometer equipped with a laboratory HHG EUV source for serving as a stand-alone metrology tool. We redesigned the previous scatterometer module by optimizing the adjustable distance of sample to detector to give rise to more diffraction orders of scattering from nanoscale structures. This allows both the $m = +1$ and -1 diffracted beams to be directly and simultaneously collected by the CCD camera with maximal spatial resolution. We rescale the measured diffraction intensity data by $1 + x_i^2/R^2$ to map the flat detector coordinate back to the Ewald sphere in which keeps the propagation distance of each harmonic from sample to the detector planes uniformly equal. One advantage of using the ratios of the $m = +1$ and

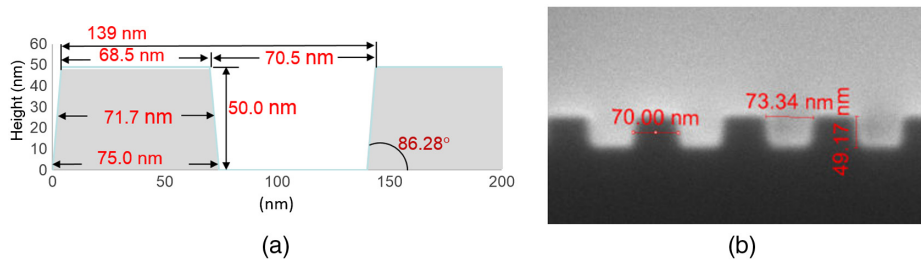


Fig. 5 (a) Reconstructed grating profile based on the best-match results for parameters including top CD, bottom CD, and grating depth. (b) Cross-sectional SEM image.

-1 diffracted intensities of each harmonics for matching analysis is that any changes in the grating target parameters due to EUV source fluctuations essentially cancel out. This contributes toward the potential robustness of the electromagnetic modeling-based metrology approach. The above innovative approach involves the accurate extraction of grating profile by finding the best match between the corrected experimental data and predetermined theoretical results stored in a library.

Although the current test sample is a 140-nm pitch, 72-nm wide grating structure (smallest current sample grating width available for purchasing) and fits to a simple single trapezoid model, this might be characterized with a conventional OCD tool. Considering the substantial challenges of future applications due to decreasing dimensions and complex 3-D structures (FinFET, Nanowire, etc.) employing higher order harmonics at nonzerth orders opens up a potential metrology solution to complement conventional scatterometers. In the near future, we plan to integrate an optical microscope module for viewing and identifying the region to be examined so that any pattern position on the specimen, even just a few microns, can be easily found. A large field-of-view CCD camera, offering two times wider imaging area comparing to our current one will be used for small pitch structure applications. We will refine our current profile model by introducing a varying complex refractive index for material applications. Other parameters, such as round corners, linewidth and line-edge roughness, and local variations in the period structures, will be considered. We will optimize the library search method to reduce the matching time. The presented data form a preliminary set of results, and a more detailed uncertainty analysis will be performed in the future.

Acknowledgments

This work was supported by the Ministry of Economic Affairs (MOEA, Grant No. 105-EC-17-A-01-05-0337) and the Advanced Technology Project within the Industrial Technology Research Institute. The authors would like to thank Professor Chen's team, Extreme UltraViolet/National Tsing Hua University (EUV/NTHU), for providing the EUV source and valuable discussions with respect to EUV applications. The authors would also like to thank

Professor Chu of National Central University for kindly offering us the x-ray CCD to collect the appropriate diffraction pattern.

References

1. P. C. Logofătu, "UV scatterometry," *Proc. SPIE* **5038**, 208–214 (2003).
2. H. T. Huang and F. L. Terry Jr., "Spectroscopic ellipsometry and reflectometry from gratings (scatterometry) for critical dimension measurement and in situ, real-time process monitoring," *Thin Solid Films* **455–456**, 828–836 (2004).
3. R. A. Bartels et al., "Generation of spatially coherent light at extreme ultraviolet wavelengths," *Science* **297**(5580), 376–378 (2002).
4. M. C. Chen et al., "Generation of bright isolated attosecond soft x-ray pulses driven by multicycle midinfrared lasers," *Proc. Natl. Acad. Sci. U. S. A.* **111**(23), E2361–E2367 (2014).
5. T. K. Gaylord and M. G. Moharam, "Analysis and applications of optical diffraction by gratings," *Proc. IEEE* **73**(5), 894–937 (1985).
6. N. Chateau and J. Hugonin, "Algorithm for the rigorous coupled wave analysis of grating diffraction," *J. Opt. Soc. Am. A* **11**(4), 1321–1331 (1994).
7. Y. S. Ku et al., "EUV scatterometer with a high-harmonic-generation EUV source," *Opt. Express* **24**(24), 28014–28025 (2016).
8. E. Lorek et al., "High-order harmonic generation using a high-repetition-rate turnkey laser," *Rev. Sci. Instrum.* **85**, 123106 (2014).
9. Y. Nagata et al., "Development of coherent EUV scatterometry microscope with high-order harmonic for EUV mask inspection," *Proc. SPIE* **8849**, 884914 (2013).
10. H. W. Sun et al., "Extended phase matching of high harmonic generation driven by plasma-induced defocusing," *Optica* **4**(8), 976–981 (2017).
11. M. G. Moharam et al., "Formulation for stable and efficient implementation of the rigorous coupled-wave analysis of binary gratings," *J. Opt. Soc. Am. A* **12**(5), 1068–1076 (1995).
12. S. Peng and G. M. Morris, "Efficient implementation of rigorous coupled-wave analysis for surface relief gratings," *J. Opt. Soc. Am. A* **12**(5), 1087–1096 (1995).
13. D. F. Gardner et al., "High numerical aperture reflection mode coherent diffraction microscopy using off-axis apertured illumination," *Opt. Express* **20**(17), 19050–19059 (2012).

Yi-Sha Ku received her BS degree in physics in 1985 from National Central University and a PhD in nuclear science from National Tsing Hua University, Taiwan, in 1992. She is currently a senior principal researcher at ITRI and a professor at the National Tsing Hua University. Previously, she worked with the National Measurement Laboratory for 11 years and was responsible for the development of primary quantum metrology standards. She has 10 years of experience in the field of overlay metrology and was engaged in model-based method and analysis algorithms. Her current research interests involve developing metrology solutions for 3-D interconnect processes.

Biographies for the other authors are not available.